Integrated Vehicle Dynamics Control Via Torque Vectoring Differential and Electronic Stability Control to Improve Vehicle Handling and Stability Performance

Seyed Mohammad Mehdi Jaafari[1]
Mechanical Engineering Department,
Faculty of Engineering,
Shahid Chamran University of Ahvaz,
Ahvaz 6135743337, Iran
e-mail: smm.jaafari@yahoo

Kourosh Heidari Shirazi
Professor
Mechanical Engineering Department,
Faculty of Engineering,
Shahid Chamran University of Ahvaz,
Ahvaz 6135743337, Iran
e-mail: k.shirazi@scu.ac.ir

This paper proposed a full vehicle state estimation and developed an integrated chassis control by coordinating electronic stability control (ESC) and torque vectoring differential (TVD) systems to improve vehicle handling and stability in all conditions without any interference. For this purpose, an integrated TVD/ESC chassis system has been modeled in MATLAB/SIMULINK *and applied into the vehicle dynamics model of the 2003 Ford Expedition in* CARSIM *software. TVD is used to improve handling in routine and steady-state driving conditions and ESC is mainly used as the stability controller for emergency maneuvers or when the TVD cannot improve vehicle handling. By the $\beta - \dot{\beta}$ phase plane, vehicle stable region is determined. Inside the reference region, the handling performance and outside the region the vehicle stability has been in question. In order to control the integrated chassis system, a unified controller with three control layers based on fuzzy control strategy, $\beta - \dot{\beta}$ phase plane, longitudinal slip, and road friction coefficient of each tire is designed in* MATLAB/SIMULINK. *To detect the control parameters, a state estimator is developed based on unscented Kalman filter (UKF). Bees algorithm (BA) is employed to optimize the fuzzy controller. The performance and robustness of the integrated chassis system and designed controller were conformed through routine and extensive simulations. The simulation results via a co-simulation of* MATLAB/SIMULINK *and CarSim indicated that the designed integrated ESC/TVD chassis control system could effectively improve handling and stability in all conditions without any interference between subsystems.* [DOI: 10.1115/1.4038657]

Keywords: handling, stability, unscented Kalman filter, phase plane method, torque vectoring systems

1 Introduction

Nowadays, active vehicle systems have a significant role in improving vehicle safety and handling and reducing fatal crashes. Nevertheless, there is no single system that can be effective over the entire range of vehicle handling and stability. So, the simultaneous presence of various stand-alone control systems on a single vehicle is essential to keep the vehicle stable and under control at all times [1]. Besides, designing a proper control system is needed to coordinate interactions between these systems to improve vehicle performance and to avoid their interferences. On the other hand, effective operation of each of these systems depends on an accurate knowledge of the vehicle states, such as velocity, lateral acceleration, yaw rate, as well as vehicle side-slip and tire friction [2]. Therefore, measuring or estimating these parameters is very vital for the designed controller.

In recent years, braking forces distribution with the electronic stability control system (ESC) and traction forces distribution with torque vectoring differential (TVD) are extensively applied in the new brands of the car producers [3–5]. TVDs has a great performance in handling events in steady-state conditions and ESC is more effective to improve stability in critical and emergency situations while the TVDs cannot induce the vehicle instability in these events [6]. However, a weak point of ESC is speed and longitudinal acceleration reduction due to braking [7]. Therefore, an integration of both systems can be a solution to achieve improved overall vehicle performance in handling and stability.

Many papers have been published in the area of active safety systems integration in an effort to improve the vehicle stability and handling. He et al. [8] proposed integration of active front steering (AFS) and dynamic stability control to achieve improvement of vehicle stability and handling performance. The AFS controller is designed to improve vehicle steerability and the dynamic stability control controller is formulated to maintain vehicle stability. Cooper [9] focused on the integration of roll moment distribution control and variable torque distribution control to improve vehicle handling and dynamics. Goodarzi and Alirezaie [10] designed an integrated fuzzy/optimal AFS/ direct yaw moment control controller based on optimal LQR control strategies; each one has been designed for a specific driving condition. Song [1] developed, evaluated, and compared four integrated dynamics control systems abbreviated as integrated dynamics control with four wheel brake, integrated dynamics control with front steering, integrated dynamics control with rear steering, and integrated dynamics control with four wheel steering. In this paper, a fuzzy logic controller and a sliding mode ABS controller were used. Jaafari and Shirazi [4] made a comparison on different torque vectoring strategies, to find

[1]Corresponding author.

Contributed by the Dynamic Systems Division of ASME for publication in the JOURNAL OF DYNAMIC SYSTEMS, MEASUREMENT, AND CONTROL. Manuscript received February 3, 2017; final manuscript received December 1, 2017; published online January 16, 2018. Assoc. Editor: Junmin Wang.

Copyright © 2018 by ASME

Downloaded From: https://dynamicsystems.asmedigitalcollection.asme.org on 11/20/2018 Terms of Use: http://www.asme.org/about-asme/terms-of-use

the best strategy in terms of improving handling, fuel consumption, stability, and ride comfort performances. According to the results, the stationary clutch torque vectoring differential (STC-TVD) shows better handling compare to ESC, while ESC is more effective in improving the stability in critical situation.

However, none of these papers argued about parameters that are difficult to measure directly and should be estimated and also they do not discuss the technical details of controller operation in different conditions like unexpected conditions, very slippery surfaces, or μ split road condition.

This paper proposes a full state estimation in a four wheel drive (4WD) vehicle and designs a complete control algorithm to divide the duties and coordinate interactions between ESC and TVD systems in order to improve vehicle performance in handling and stability at all times while minimizing the effects of any disturbances. The paper is organized as follows: In Sec. 2, the vehicle model is discussed. In Sec. 3, torque vectoring systems are introduced. In Sec. 4, the controller is designed. In Sec. 5, the state estimation procedure is presented. Bees algorithm (BA) is used as fuzzy rules and membership function optimization in Sec. 6. In Sec. 7, simulation results are shown. Finally, in Sec. 8, concluding remarks are presented.

2 Nonlinear Vehicle Model

CARSIM [11] is a software package from mechanical simulation corporation (Ann Arbor, MI), for simulating and analyzing the behavior of vehicles in response to steering, braking, acceleration inputs, and so on. It includes a database with many example vehicles and test procedures. In this paper, all simulations were performed using the fully nonlinear CarSim vehicle model. The modeled vehicle is a 2003 Ford Expedition XLT. To build a CarSim Ford 2003 model, the parameters of the vehicle are obtained from Ref. [12]. The sprung mass, wheelbase, CG location and vehicle inertias are entered in the CarSim Sprung Mass datascreen as shown in Fig. 1. The result of simulation in the Sine with Dwell maneuver [12] shows that the dynamic behavior of the CarSim Ford 2003 model is very similar to real Ford 2003 (Fig. 2).

3 Torque Vectoring Systems

3.1 The Torque Vectoring Differential. According to the great performance of STC-TVD mechanism in handling events [4,13], this system is used as the TVD system in this study. STC-TVD has two stationary clutches and two series of planetary gears, which are on the both output shafts of the ordinary differential (Fig. 3). When the left clutch is activated, more torque is transferred to the left wheel and when the right clutch is activated, more torque is transferred to the right wheel [13,14]. The demanded torque transfer to the faster wheel can be achieved if the wheel speed difference does not exceed by more than the 28% of slower wheel speed (allowable wheel speed difference). It is assumed that this system is used in the rear axle of a 4WD vehicle and an open differential is used in front axle and as the center differential. The relative speed between the left clutch plates and the relative speed between the right clutch plates are calculated from Eqs. (1) and (2), respectively. The torque transmitted to the wheels is derived from Eqs. (3)–(6), respectively (more details about this system are given in Ref. [13])

$$\omega_{f1} = H_{11}\omega_2 - H_{12}\omega_1 \tag{1}$$

$$\omega_{f2} = H_{21}\omega_1 - H_{22}\omega_2 \tag{2}$$

$$\begin{aligned} T_{tLR} = {} & \frac{1}{4} i T_e + H_{12} T_{f1} - H_{21} T_{f2} \\ & - \dot{\omega}_1 \left(I_1^* + \frac{1}{4} i^2 I_{ir}^* + H_{12}^2 I_{C1} + H_{21}^2 I_{C2} \right) \\ & - \dot{\omega}_2 \left(\frac{1}{4} i^2 I_{ir}^* - H_{11} H_{12} I_{C1} - H_{21} H_{22} I_{C2} \right) \end{aligned} \tag{3}$$

$$\begin{aligned} T_{tRR} = {} & \frac{1}{4} i T_e + H_{22} T_{f2} - H_{11} T_{f1} \\ & - \dot{\omega}_1 \left(\frac{1}{4} i^2 I_{ir}^* - H_{11} H_{12} I_{C1} - H_{21} H_{22} I_{C2} \right) \\ & - \dot{\omega}_2 \left(I_2^* + \frac{1}{4} i^2 I_{ir}^* + H_{11}^2 I_{C1} + H_{22}^2 I_{C2} \right) \end{aligned} \tag{4}$$

$$T_{tLF} = \frac{1}{4} i T_e - \frac{1}{4} i^2 I_{if}^* \dot{\omega}_4 - \dot{\omega}_3 \left(I_3 + \frac{1}{4} i^2 I_{if}^* \right) \tag{5}$$

$$T_{tRF} = \frac{1}{4} i T_e - \frac{1}{4} i^2 I_{if}^* \dot{\omega}_3 - \dot{\omega}_4 \left(I_4 + \frac{1}{4} i^2 I_{if}^* \right) \tag{6}$$

where

$$h_1 = h_2 = \frac{Z_1 Z_3}{Z_2 Z_4}, \quad H_{11} = \frac{h_1}{2(h_1 - 1)}, \quad H_{12} = \frac{2 - h_1}{2(h_1 - 1)},$$
$$H_{21} = \frac{h_2}{2(h_2 - 1)}, \quad H_{22} = \frac{2 - h_2}{2(h_2 - 1)},$$
$$I_{if}^* = I_i + i^{-2}(I_c + I_{s1} + I_{s2}), \quad I_{s2} = I_{s1}, \quad I_1^* = I_1 + I_{r1},$$
$$I_2^* = I_2 + I_{r2}, \quad I_{r2} = I_{r1}, \quad I_{ir}^* = I_i + i^{-2}(I_c)$$

T_f is the frictional torque transmitted by the clutch in TVD, which is a function of the normal compression force on each disk (F_c),

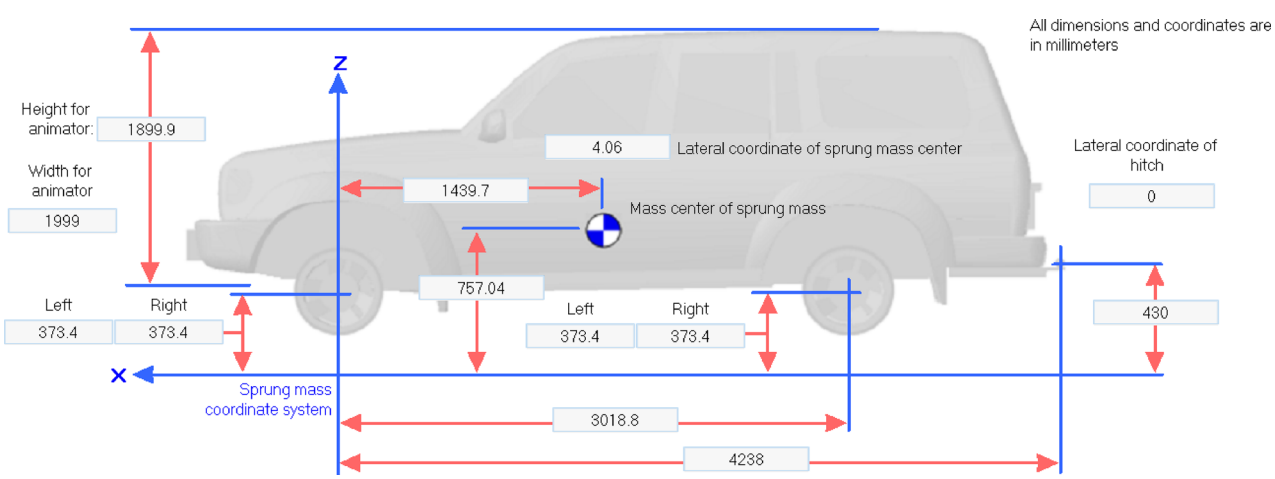

Fig. 1 Vehicle parameter in CarSim

Downloaded From: https://dynamicsystems.asmedigitalcollection.asme.org on 11/20/2018 Terms of Use: http://www.asme.org/about-asme/terms-of-use

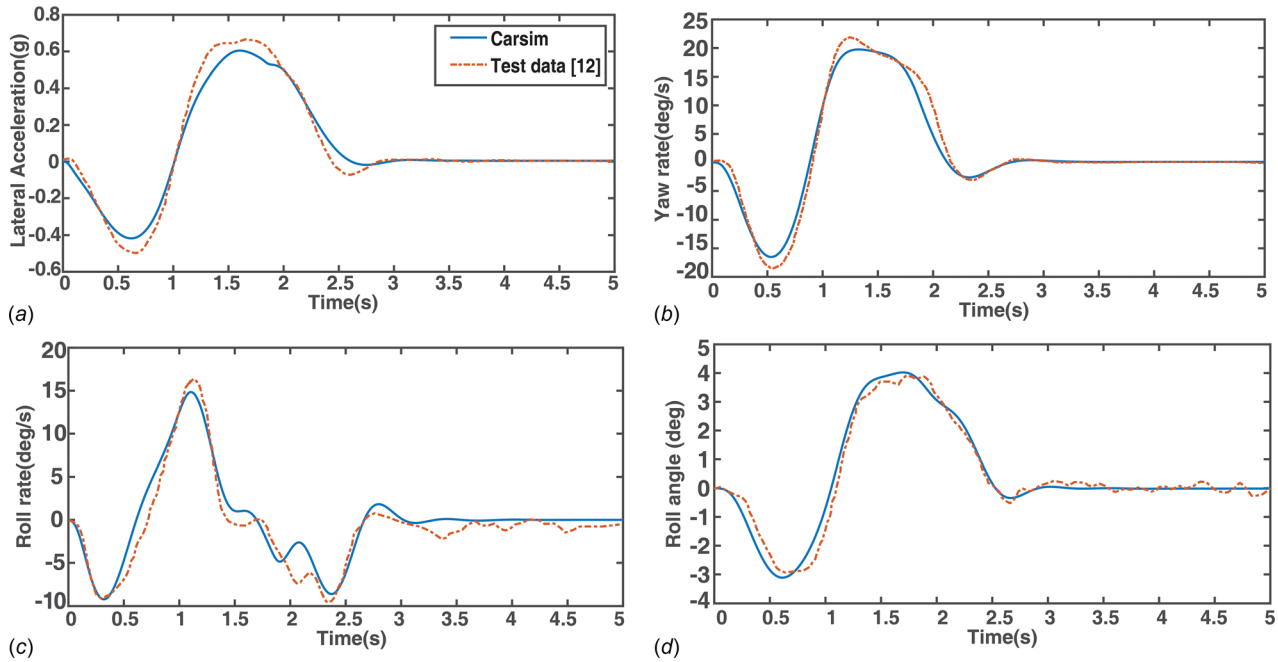

Fig. 2 The comparison of simulation results (CarSim) and field test data (Ref. [12])

number of active friction surfaces (n_c), the clutch friction surface radius (r_c), and friction coefficient (μ_F), which generally depends on the clutch's relative speed and calculated from Eq. (7) [15]

$$T_f = F_c r_c n_c \mu_F = T_{\text{req}} \mu_F \tag{7}$$

where T_{req} is hydraulic torque and (μ_F) can be described by the generalized Stribeck friction model [16]. Obviously, by choosing n_c and r_c by the designer, the force needed to push the clutch is derived from $T_{\text{req}}/n_c r_c$. A delay of 0.2 s is used as the differential actuator time lag. Also, the Karnopp clutch friction model is used for zero-speed region (locked mode) [17]. Parameters values used in the active differential are given in Appendix A.

3.2 The Electronic Stability Control System. Electronic stability control system typically utilizes solenoid-based hydraulic modulators to change the brake pressures at the four wheels. Creating differential braking by increasing the brake pressure at the left wheels compared to the right wheels, a counter-clockwise yaw moment is generated. Likewise, increasing the brake pressure at the right wheels compared to the left wheels creates a clockwise yaw moment [18]. In the understeer situation, braking force is applied on the inside rear wheel but if (1) this tire is on the threshold of locked mode, or (2) the friction in this tire is much lower than the inside front wheel or (3) when the longitudinal slip in this tire is high and in inside front wheel is low, then braking force is applied on the inside front wheel also in the situation in which $|\beta + 4\beta| > 80\mu$ (Sec. 4) with considering the locked mode, longitudinal slip, and friction—as discussed earlier—braking force is applied on the both inside wheels. The same story is applied in the oversteer situation.

4 The Integrated Control System

Handling improvement and stability control are the most important goals of every vehicle control systems. When the handling limit is approached, vehicle stability should be in question. Therefore, handling and stability are the two control objectives in this paper. It should be noted that vehicle stability control will be used only close to and at the limit of handling. As discussed in Refs. [4] and [13], TVDs have a great performance in handling events without having a significant reduction in acceleration or

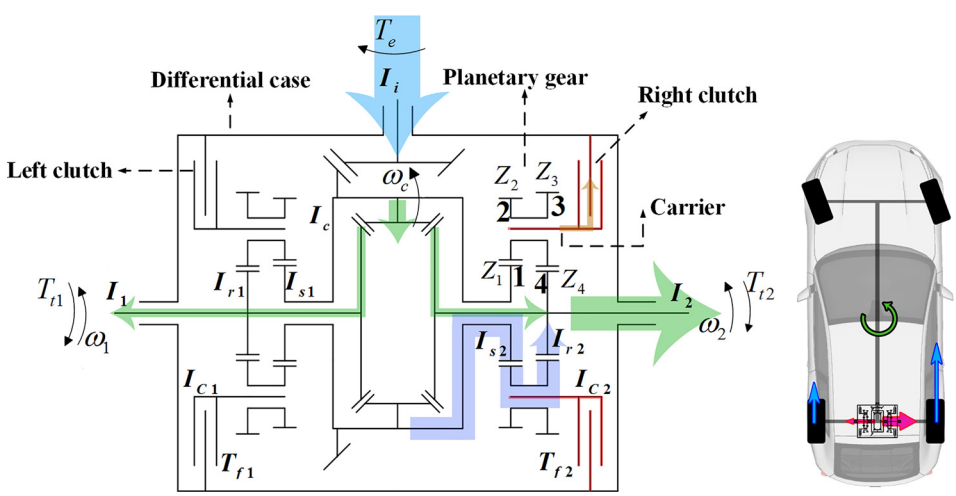

Fig. 3 Kinematic schemes of STC-TVD

Downloaded From: https://dynamicsystems.asmedigitalcollection.asme.org on 11/20/2018 Terms of Use: http://www.asme.org/about-asme/terms-of-use

longitudinal speed. On the other hand, critical and emergency situations are a weak point for TVDs while ESC shows a significant stability improvement in these conditions [4]. Therefore, in this study, TVD is used to improve handling in nearly normal and steady-state driving conditions and ESC controller is mainly used as the stability controller for emergency maneuvers or when the TVD cannot improve vehicle handling in some situation like in very slippery surfaces. Since the vehicle yaw rate and side-slip angle are deeply concerned with handling and stability, in this study, these variables will be chosen as the under control signals for the handling and dynamic stability, respectively. Due to the nature of nonlinearity and second-order property of the dominant lateral vehicle dynamics, analysis of vehicle stability can be performed using the phase-plane method. The phase-plane method is quite effective in the analysis of vehicle stability with respect to the side-slip motion [19]. The phase-plane method in the design of vehicle stability control has been found in Refs. [19–21].

Phase portrait of $\beta - \dot{\beta}$ plan under different conditions is plotted in Fig. 4. Stable and unstable trajectories are plotted in solid and dashed lines, respectively. In order to keep the vehicle safe at all times, the side-slip motion of vehicle must be bounded within a region in which the vehicle remains stable. For this purpose, a reference stable region is defined in the $\beta - \dot{\beta}$ plan. This stable region can be expressed as

$$|\dot{\beta} + K'\beta| < b' \tag{8}$$

where K' and b' are positive constants and determine the slope and the width of the region. The parameter values for dry road and zero steer input are $(K' = 4, b' = 75)$ as shown in Fig. 4(*a*). However, to guarantee the vehicle stability in other situations (Figs. 4(*b*) and 4(*c*)), these parameters are chosen more conservatively as follows (Fig. 4(*d*)):

$$|\dot{\beta} + 4\beta| < 30\mu \tag{9}$$

Inside the reference region, the handling performance while in outside the region the vehicle stability must be controlled. The perpendicular distance of the actual state from the reference region in the phase plane (ξ) is used as the error signal for the stability control loop while the yaw rate error is used for the handling control loop (Fig. 4(*d*)). Yaw rate error is defined as the difference between actual and a desired yaw rate. The desired yaw rate can be defined based on the "bicycle model" yaw motion behavior. According to Refs. [18] and [22], the "bicycle model" yaw rate is obtained from driver's steering input, and vehicle speed by the following equation:

$$r_d = \frac{v_x \delta}{(b+a) + K_u v_x^2}, \quad K_u = \frac{M}{b+a}\left(\frac{b}{C_f} - \frac{a}{C_r}\right) \tag{10}$$

Considering the tire-road friction coefficient, r_d must comply with the following conditions:

$$|r_d| < \left|\frac{\mu g}{v_x}\right| \tag{11}$$

where r_d is the desired yaw rate, C_f and C_r are the front and rear cornering stiffness, respectively, M is the vehicle mass, μ is the road friction coefficient, and (v_x) is the vehicle longitudinal speed, which is taken from vehicle model.

To avoid the interferences of different control objectives, individual subsystem should be activated according to driving situations. Therefore, in order to improve vehicle handling and stability and to achieve the above goals, a controller is proposed with three control layers. The first layer control system duties are:

(1) According to the phase plane trajectory, it chooses the appropriate control strategy between handling and stability. Inside the reference region, the handling performance and in outside the region, the vehicle stability must be controlled.
(2) According to the control strategy, longitudinal slip and road friction coefficient of each tire, it switches the appropriate torque vectoring system between ESC and TVD. The TVD will be used for handling performance and the ESC will be used for the stability and the situation in which the TVD cannot improve handling performance including; (a) very low road friction, in μ split road condition, (b) very low friction in the appropriate tire for clutching in TVD, (c) high longitudinal slip in the appropriate tire for clutching in TVD, and (d) the speed difference exceed the allowable wheel speed difference.

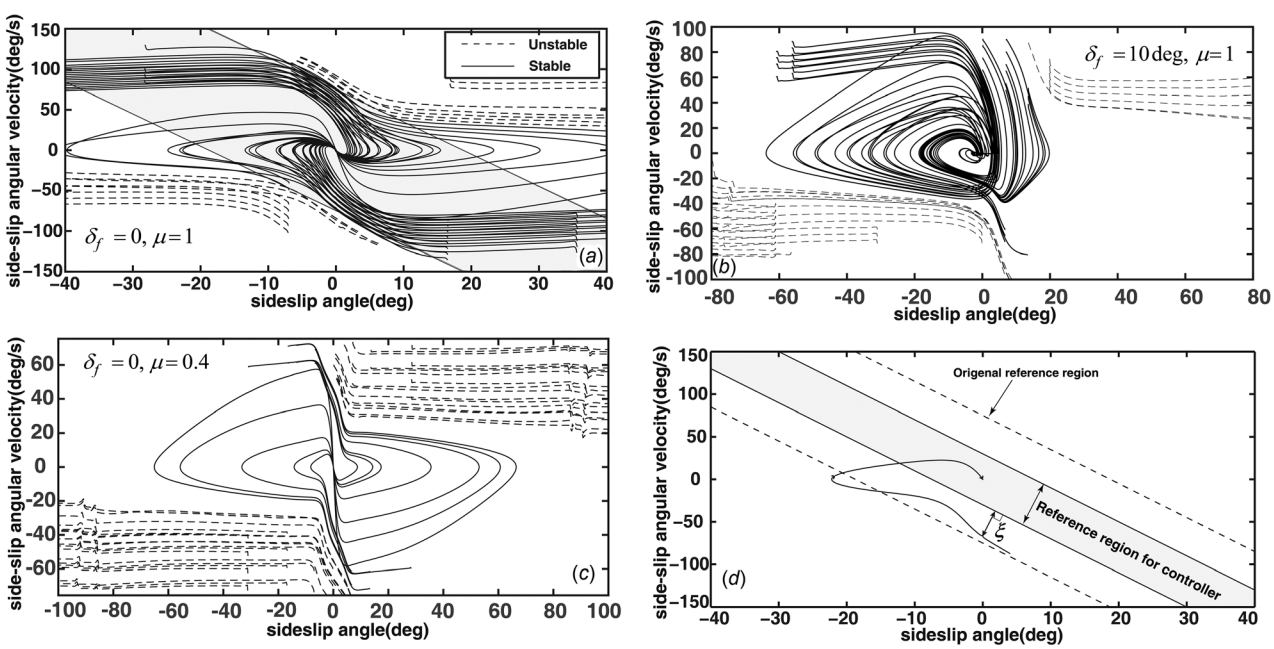

Fig. 4 Phase portrait of $\beta - \dot{\beta}$ plan

Downloaded From: https://dynamicsystems.asmedigitalcollection.asme.org on 11/20/2018 Terms of Use: http://www.asme.org/about-asme/terms-of-use

The second layer control system is a fuzzy-based controller. The advantages of fuzzy methods are their simplicity, easy implementing, fast response, and inherent robustness in controlling nonlinear systems. For stability performance, the fuzzy inputs are the perpendicular distance of vehicle state from the reference region in the phase plane ($\varepsilon_{\beta\dot{\beta}} = \xi \mathrm{sign}(\dot{\beta} + 4\beta)$) and its derivative ($\dot{\varepsilon}_{\beta\dot{\beta}}$) and the fuzzy output is T_B. For handling performance, the fuzzy inputs are yaw rate error ($e = r - r_d$) and its derivative ($\dot{e} = \dot{r} - \dot{r}_d$) and output is T_{req} (Eq. (7)). To prevent the tire from spinning on slippery surfaces, the fuzzy output should be modulated according to the road friction coefficient of each tire. The vehicle yaw rate (r) is taken from vehicle model and the side-slip angle; longitudinal slip and road friction coefficient of each tire are estimated from the measured vehicle states.

The third layer control system roles are:

(1) Checking the allowable wheel speed difference for TVD to prevent the wrong torque distribution direction, and checking the wheel speed to prevent the tire from becoming locked in ESC system.
(2) Switches the appropriate clutching in TVD or appropriate tires for braking in ESC according to the selective torque control system (ESC or TVD), longitudinal slip and road friction coefficient of each tire, vehicle state in phase plane

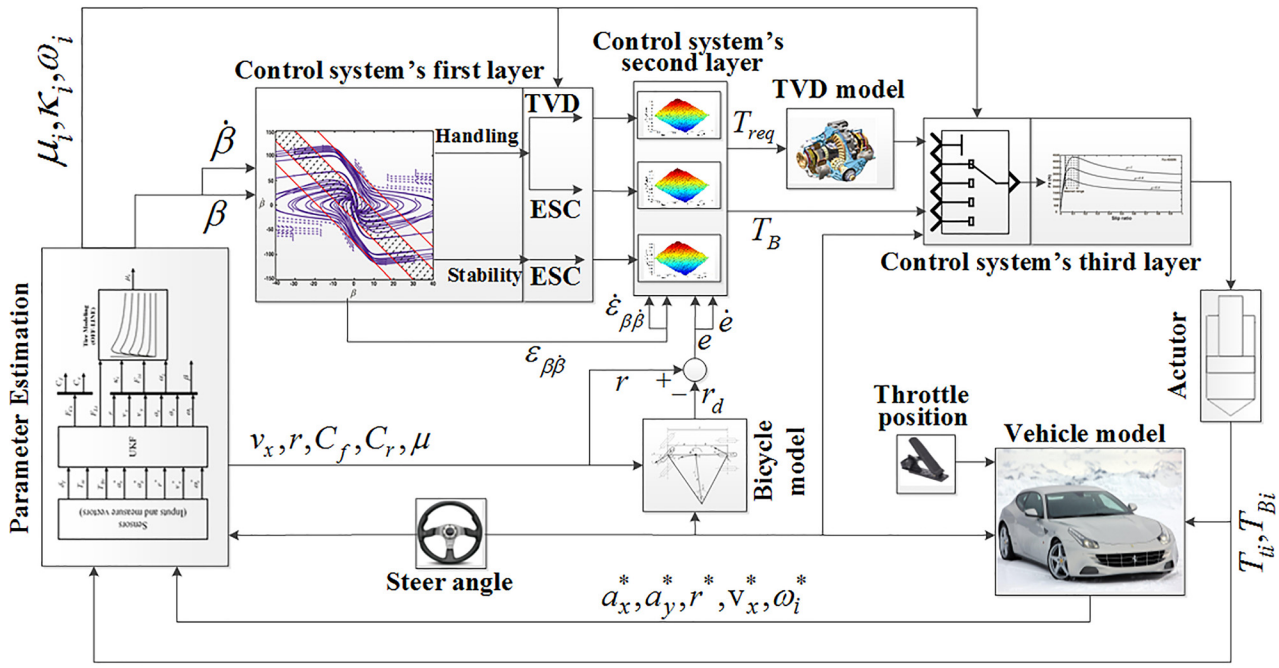

(*a*)

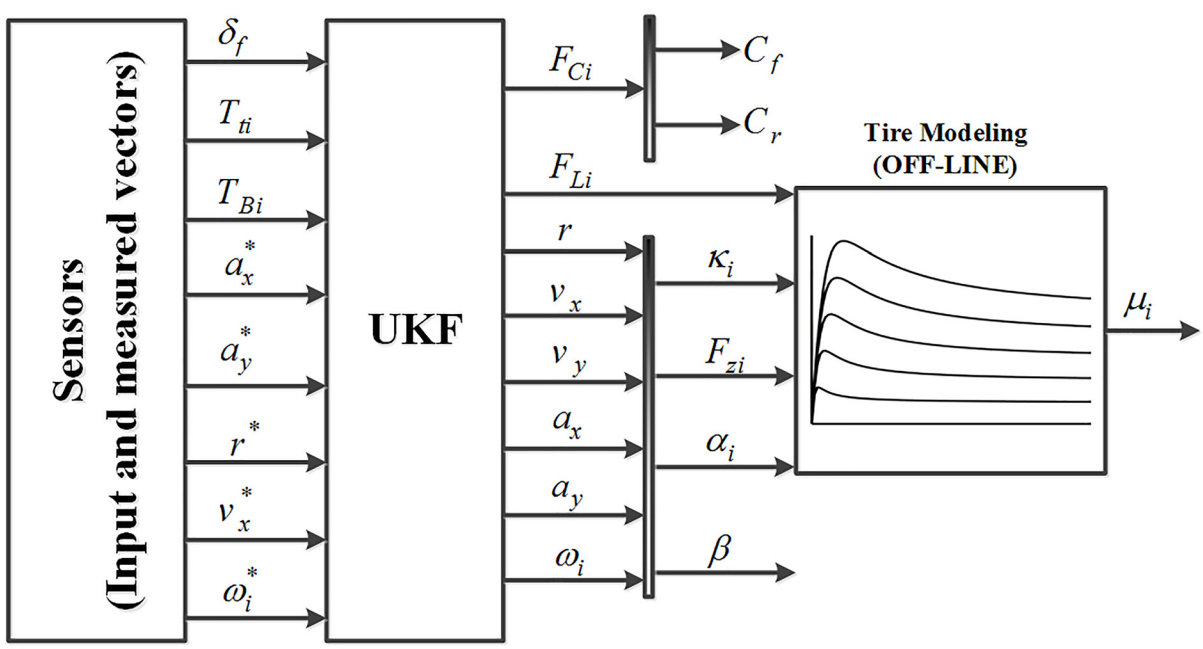

(*b*)

Fig. 5 (*a*) Schematic of control system and (*b*) structure of state estimator

Downloaded From: https://dynamicsystems.asmedigitalcollection.asme.org on 11/20/2018 Terms of Use: http://www.asme.org/about-asme/terms-of-use

method—particularly for stability region—and oversteer or understeer conditions.

The schematic diagram of the control system is depicted in Fig. 5(*a*). The performance of the controller in selecting the appropriate clutching or braking, input and output normalized membership functions and fuzzy rules used to control the torque control systems, along with abbreviations used in fuzzy rules and membership functions are given in Appendix B.

5 Parameter Estimation

From Sec. 4, it is shown that the values of yaw rate, vehicle side-slip, longitudinal slip, and road friction coefficient of each tire are necessary for controller. Yaw rate can be measured by yaw rate sensor but since sensors for the direct measurement of side-slip angle, road friction coefficient, and longitudinal slip are limited or unavailable, they should be estimated from the measured vehicle states. In this study, the proposed state estimators are developed based on the unscented Kalman filter (UKF), which is robust and has a high-speed of convergence [23].

5.1 Nonlinear Observer. Since the individual wheel information is needed for vehicle control system in this paper, a simple and sufficient 4WD vehicle model is used for vehicle state estimation. The model comprises longitudinal, lateral, and yaw motions and ignores heave, roll, and pitch motions. Nonlinear dynamic equations of this model can be expressed as follows:

$$\dot{v}_x = rv_y + \frac{1}{m}\left((F_{\mathrm{LRF}} + F_{\mathrm{LLF}})\cos(\delta_f) - F_{\mathrm{CF}}\sin(\delta_f) + F_{\mathrm{LLR}} + F_{\mathrm{LRR}}\right) \tag{12}$$

$$\dot{v}_y = -rv_x + \frac{1}{m}\left((F_{\mathrm{LLF}} + F_{\mathrm{LRF}})\sin(\delta_f) + F_{\mathrm{CF}}\cos(\delta_f) + F_{\mathrm{CR}}\right) \tag{13}$$

$$\dot{r} = \frac{1}{I_z}\left(\left((F_{\mathrm{LRF}} - F_{\mathrm{LLF}})\frac{t}{2} + aF_{\mathrm{CF}}\right)\cos(\delta_f) + (F_{\mathrm{LRR}} - F_{\mathrm{LLR}})\frac{t}{2} + a(F_{\mathrm{LLF}} + F_{\mathrm{LRF}})\sin(\delta_f) - bF_{\mathrm{CR}}\right) \tag{14}$$

$$a_x = \frac{1}{m}\left((F_{\mathrm{LLF}} + F_{\mathrm{LRF}})\cos(\delta_f) - F_{\mathrm{CF}}\sin(\delta_f) + F_{\mathrm{LLR}} + F_{\mathrm{LRR}}\right) \tag{15}$$

$$a_y = \frac{1}{m}\left((F_{\mathrm{LLF}} + F_{\mathrm{LRF}})\sin(\delta_f) + F_{\mathrm{CF}}\cos(\delta_f) + F_{\mathrm{CR}}\right) \tag{16}$$

$$\dot{\omega}_i = \frac{1}{I_w}(T_i - R_w F_{Li}), i = \mathrm{LF, LR, RF, RR} \tag{17}$$

where $F_{\mathrm{CF}} = F_{\mathrm{CLF}} + F_{\mathrm{CRF}}$ and $F_{\mathrm{CR}} = F_{\mathrm{CLR}} + F_{\mathrm{CRR}}$.

The steering angle, longitudinal and lateral accelerations, four-wheel speeds, engine torque, braking torque, and longitudinal vehicle speed are measured from sensors mounted on the vehicle—although they are noisy and need to be filter—and other state information are estimated by UKF.

In general, a discrete-time nonlinear state space system can be formulated as

$$\begin{aligned} \mathbf{x}_k &= f(x_{k-1}, u_{k-1}, w_{k-1}) \\ \mathbf{y}_k &= h(x_k, u_k, v_k) \end{aligned} \tag{18}$$

where f is the state prediction function, h is the observation function, $\mathbf{x}$ is the state vector, $\mathbf{y}$ is the output vector, u is the input vector, with $\mathbf{w}$ and $\mathbf{v}$ being the process noise and measurement noise vectors, respectively, and $\mathbf{k}$ is the discrete-time index.

The input vector $\mathbf{u}$ includes the steering wheel angle and driving and braking torques of tires

$$\mathbf{u} = [\delta_f, T_{t\mathrm{LF}}, T_{t\mathrm{RF}}, T_{t\mathrm{LR}}, T_{t\mathrm{RR}}, T_{\mathrm{BLF}}, T_{\mathrm{BRF}}, T_{\mathrm{BLR}}, T_{\mathrm{BRR}}] \tag{19}$$

By measuring the engine torque (T_e) and calculating the T_F—according to the fuzzy output (T_{req}) and from Eq. (7)—the driving torques are calculated from Eqs. (3)–(6), respectively.

The measure vector y includes longitudinal and lateral accelerations, yaw rate, longitudinal velocity, and wheel speeds

$$\mathbf{y} = [a_x, a_y, r, v_x, \omega_{\mathrm{LF}}, \omega_{\mathrm{RF}}, \omega_{\mathrm{LR}}, \omega_{\mathrm{LRR}}] \tag{20}$$

The state vector $\mathbf{x}$ includes longitudinal tire forces, lateral tire forces, yaw rate, and longitudinal and lateral velocity at CG, wheel speeds and longitudinal and lateral acceleration

$$\mathbf{x} = [F_{\mathrm{LLF}}, F_{\mathrm{LRF}}, F_{\mathrm{LLR}}, F_{\mathrm{LRR}}, F_{\mathrm{CF}}, F_{\mathrm{CR}}, r, v_x, v_y, \omega_{\mathrm{LF}}, \omega_{\mathrm{RF}}, \omega_{\mathrm{LR}}, \omega_{\mathrm{LRR}}, a_x, a_y] \tag{21}$$

Via the estimated parameters, vehicle side-slip angle (β), tire slip angle (α_i), longitudinal slip ratio (κ_i), and vertical tire forces (F_{Zi}) are given as follows:

$$\beta = \tan^{-1}\left(\frac{v_y}{v_x}\right) \tag{22}$$

$$\begin{aligned} \alpha_{\mathrm{LF}} &= \tan^{-1}\left(\frac{v_y + ra}{v_x - rt/2}\right) - \delta_f, \alpha_{\mathrm{LR}} = \tan^{-1}\left(\frac{v_y - rb}{v_x - rt/2}\right), \\ \alpha_{\mathrm{RF}} &= \tan^{-1}\left(\frac{v_y + ra}{v_x + rt/2}\right) - \delta_f, \alpha_{\mathrm{RR}} = \tan^{-1}\left(\frac{v_y - rb}{v_x + rt/2}\right) \end{aligned} \tag{23}$$

$$\kappa_i = \frac{R_{wi}\omega_i - U_{wi}}{\max(U_{wi}, R_{wi}\omega_i)}, i = \mathrm{LF, LR, RF, RR}$$
$$\left[\begin{aligned} \mathrm{U_{WRF}} &= \left(v_x + r \times \frac{\mathrm{t}}{2}\right)\cos(\delta) + (v_y + r \times a)\sin(\delta_f), \mathrm{U_{WLR}} = \left(v_x - r \times \frac{\mathrm{t}}{2}\right) \\ \mathrm{U_{WLF}} &= \left(v_x - r \times \frac{\mathrm{t}}{2}\right)\cos(\delta) + (v_y + r \times a)\sin(\delta_f), \mathrm{U_{WRR}} = \left(v_x + r \times \frac{\mathrm{t}}{2}\right) \end{aligned}\right] \tag{24}$$

$$\begin{aligned} F_{ZLF} &= \frac{mgb}{2(a+b)} - \frac{ma_x h}{2(a+b)} - \frac{ma_y h}{2t}, F_{ZRF} = \frac{mgb}{2(a+b)} - \frac{ma_x h}{2(a+b)} + \frac{ma_y h}{2t} \\ F_{ZLR} &= \frac{mga}{2(a+b)} + \frac{ma_x h}{2(a+b)} - \frac{ma_y h}{2t}, F_{ZRR} = \frac{mga}{2(a+b)} + \frac{ma_x h}{2(a+b)} + \frac{ma_y h}{2t} \end{aligned} \tag{25}$$

Downloaded From: https://dynamicsystems.asmedigitalcollection.asme.org on 11/20/2018 Terms of Use: http://www.asme.org/about-asme/terms-of-use

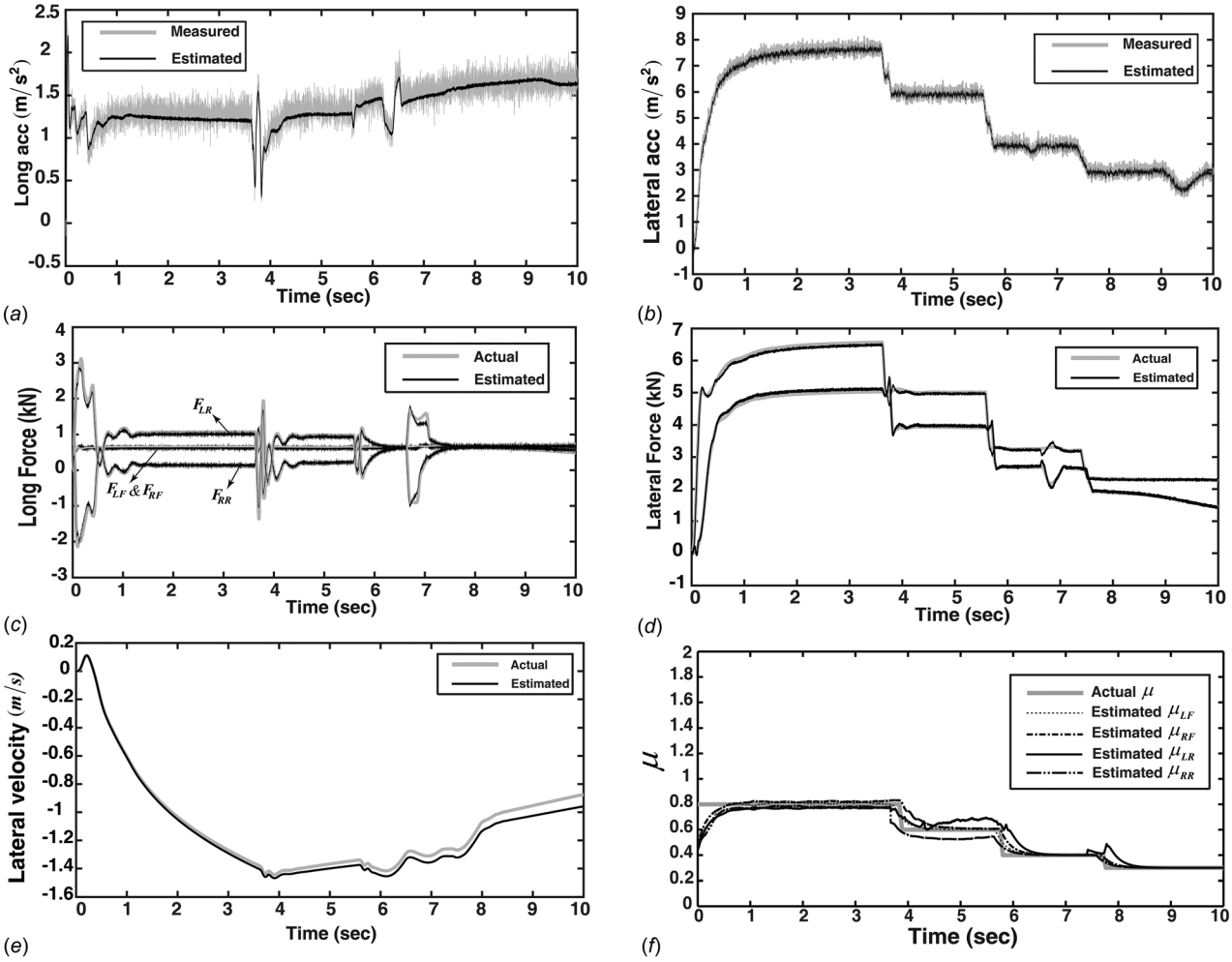

Fig. 6 Actual and estimated parameters

The desired yaw rate in Eq. (10) has been taken into account based on the assumption that the tires are linear as follows:

$$F_{CF} = C_f \alpha_F, \quad F_{CR} = C_R \alpha_R$$
$$\alpha_F = \beta + \frac{r}{v_x} a - \delta_f, \quad \alpha_R = \beta - \frac{r}{v_x} b \tag{26}$$

Therefore, after estimating lateral forces and vehicle side-slip angle, cornering stiffness can be determined by means of Eq. (26). Finally, tire road friction coefficient can be estimated recursively by statistically comparing the longitudinal forces estimated by the UKF to those obtained from the Pacejka tire model [24] for a particular μ. The schematic diagram of vehicle parameters estimation is shown in Fig. 5(*b*), where $\square^*$ is a noisy measured parameter.

5.2 The Unscented Kalman Filter. However, the extended Kalman filter is a standard and popular algorithm for optimal state estimation of nonlinear systems—by using Taylor Expansion theory and first-order approximation to linearize the nonlinear system—but for the strong nonlinear systems, it performs badly and it is difficult to calculate the Jacobi matrix [25]. In order to overcome these problems, the UKF, which is based on the unscented transformation, is proposed. Unscented transformation is a new, novel method for calculating the statistics of a random variable, which undergoes a nonlinear transformation [25]. In this method, a set of points (or sigma points) are chosen to calculate

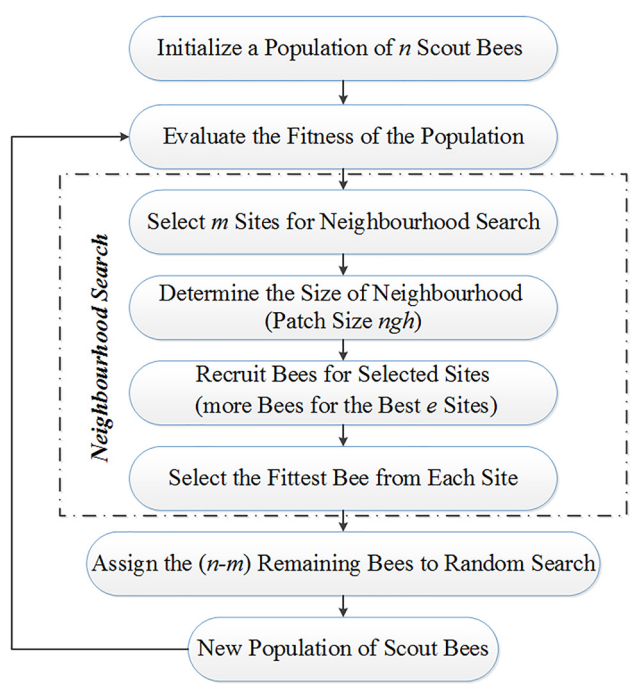

Fig. 7 Flowchart of BA algorithm

Downloaded From: https://dynamicsystems.asmedigitalcollection.asme.org on 11/20/2018 Terms of Use: http://www.asme.org/about-asme/terms-of-use

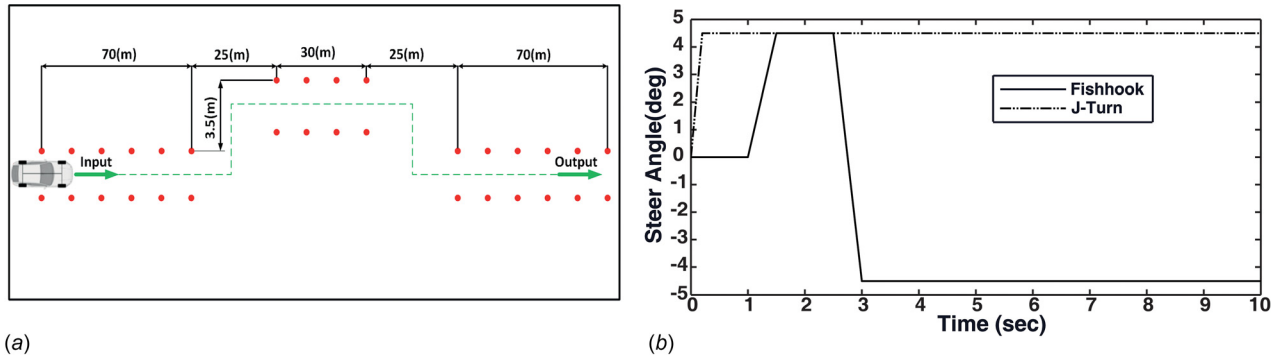

Fig. 8 (*a*) Desired path in double lane change (DLC) maneuver and (*b*) steering change in front wheels in J and fishhook

the means and covariances used in the Kalman filter. The UKF algorithm is summarized as follows [26]:

(a) Before executing filter (complete each step once before filtering):

1- Define Scaling Parameters and Weight Vectors

$$\alpha, \beta, \kappa \,(\text{default } \alpha = 1, \beta = 2, \kappa = 0)$$
$$L = n_x \,(\text{length of state vector})$$
$$\lambda = \alpha^2(L + \kappa) - L$$
$$\eta_0^m = \lambda/(L + \lambda)$$
$$\eta_0^c = \lambda/(L + \lambda) + 1 - \alpha^2 + \beta$$
$$\eta_i^m = \eta_i^c = 1/[2(L + \lambda)], i = 1, .., 2L$$

2- Determine Noise Assumptions

The process and measurement noise covariance terms are considered to be uncorrelated, white, and Gaussian with zero mean and known covariance matrices Q and R, respectively.

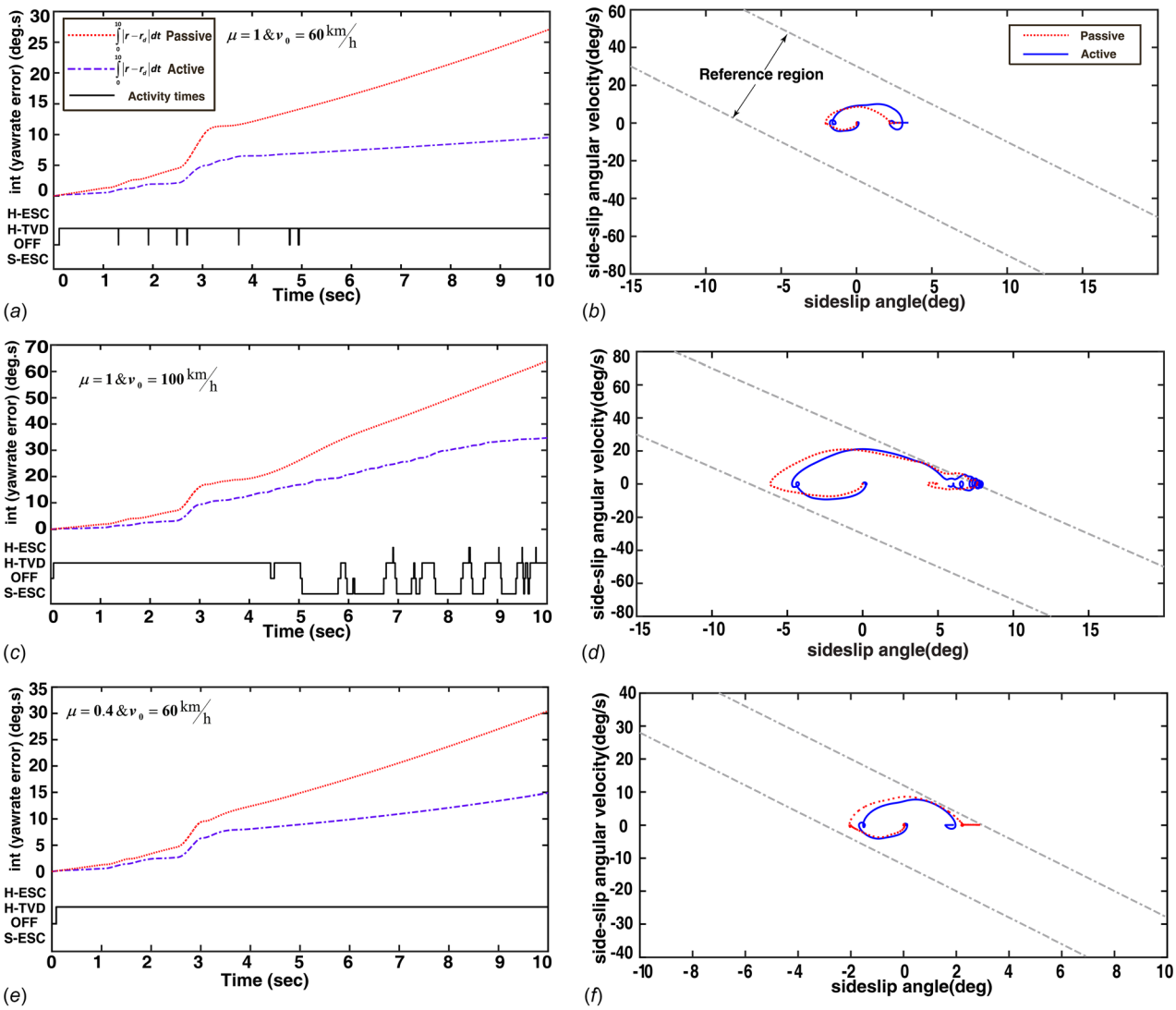

Fig. 9 Yaw rate error and the $\beta - \dot{\beta}$ phase trajectory in the phase plane in fishhook maneuver

Downloaded From: https://dynamicsystems.asmedigitalcollection.asme.org on 11/20/2018 Terms of Use: http://www.asme.org/about-asme/terms-of-use

$$\mathbf{Q}_k = E[\mathbf{w}_k \mathbf{w}_k^T],\ \mathbf{R}_k = E[\mathbf{v}_k \mathbf{v}_k^T]$$

$$Q = \mathrm{diag}([10^4, 10^4, 10^4, 10^4, 10^3, 10^3, 10^{-9}, 10^{-9}, 10^{-9}, 10^{-9}, 10^{-9}, 10^{-9}, 10^{-9}, 10^{-9}])$$
$$R = \mathrm{diag}([10^{-4}\ 10^{-4}\ 10^{-6}\ 10^{-6}\ 10^{-6}\ 10^{-6}\ 10^{-6}\ 10^{-6}])$$

3-Initialization

It is assumed that the initial state, $\hat{\mathbf{x}}_0$, is known with corresponding uncertainty given by the initial error covariance matrix, $\mathbf{P}_0$

$$\hat{\mathbf{x}}_0 = E[\mathbf{x}_0], \mathbf{P}_0 = E[(\mathbf{x}_0 - \hat{\mathbf{x}}_0)(\mathbf{x}_0 - \hat{\mathbf{x}}_0)^T]$$
$$\hat{\mathbf{x}}_0 = [600, 600, 600, 600, 0, 0, 0, \mathrm{v}_0, 0, \mathrm{v}_0/\mathrm{R}w, \mathrm{v}_0/\mathrm{R}w, \mathrm{v}_0/\mathrm{R}w, \mathrm{v}_0/\mathrm{R}w, 0, 0]$$
$$\mathbf{P}_0 = 10^{-3} \times \mathrm{diag}([1, 1, 1, 1, 0.1, 0.1, 1, 1, 1, 1, 1, 1, 1, 1, 1])$$

(b) Executing the filter recursively (perform each step at each discrete-time)

1- Generate the Sigma-Points

$$\sqrt{\mathbf{P}_{k-1}} = chol(\mathbf{P}_{k-1})\ (\text{lower Cholesky decomposition})$$
$$\boldsymbol{\chi}_{k-1} = \left[\hat{\mathbf{x}}_{k-1} \quad \hat{\mathbf{x}}_{k-1} + \sqrt{L+\lambda}\sqrt{\mathbf{P}_{k-1}} \quad \hat{\mathbf{x}}_{k-1} - \sqrt{L+\lambda}\sqrt{\mathbf{P}_{k-1}}\right]$$

2- Prediction Transformation

$$\boldsymbol{\chi}_{k|k-1}^{(i)} = \mathbf{f}\,(\boldsymbol{\chi}_{k-1}^{(i)}, \mathbf{u}_{k-1}),\ \mathrm{i} = 0, 1, .., 2L$$
$$\hat{\mathbf{x}}_{k|k-1} = \sum_{i=0}^{2L} \boldsymbol{\eta}_i^m \boldsymbol{\chi}_{k|k-1}^{(i)}$$

$$\mathbf{P}_{k|k-1} = \mathbf{Q}_{k-1} + \sum_{i=0}^{2L} \boldsymbol{\eta}_i^c (\boldsymbol{\chi}_{k|k-1}^{(i)} - \hat{\mathbf{x}}_{k|k-1})(\boldsymbol{\chi}_{k|k-1}^{(i)} - \hat{\mathbf{x}}_{k|k-1})^T$$

3- Observation Transformation

$$\boldsymbol{\psi}_{k|k-1}^{(i)} = \mathbf{h}\,(\boldsymbol{\chi}_{k|k-1}^{(i)}, \mathrm{u}_k),\ \mathrm{i} = 0, 1, .., 2L$$
$$\hat{\mathbf{y}}_{k|k-1} = \sum_{i=0}^{2L} \boldsymbol{\eta}_i^m \boldsymbol{\psi}_{k|k-1}^{(i)}$$

4- Measurement Update

$$\mathbf{K}_k = \mathbf{P}_k^{xy} (\mathbf{P}_k^{yy})^{-1}$$
$$\hat{\mathbf{x}}_k = \hat{\mathbf{x}}_{k|k-1} + \mathbf{K}_k (\mathbf{y}_k - \hat{\mathbf{y}}_{k|k-1})$$
$$\mathbf{P}_k = \mathbf{P}_{k|k-1} - \mathbf{K}_k \mathbf{P}_k^{yy} \mathbf{K}_k^T$$

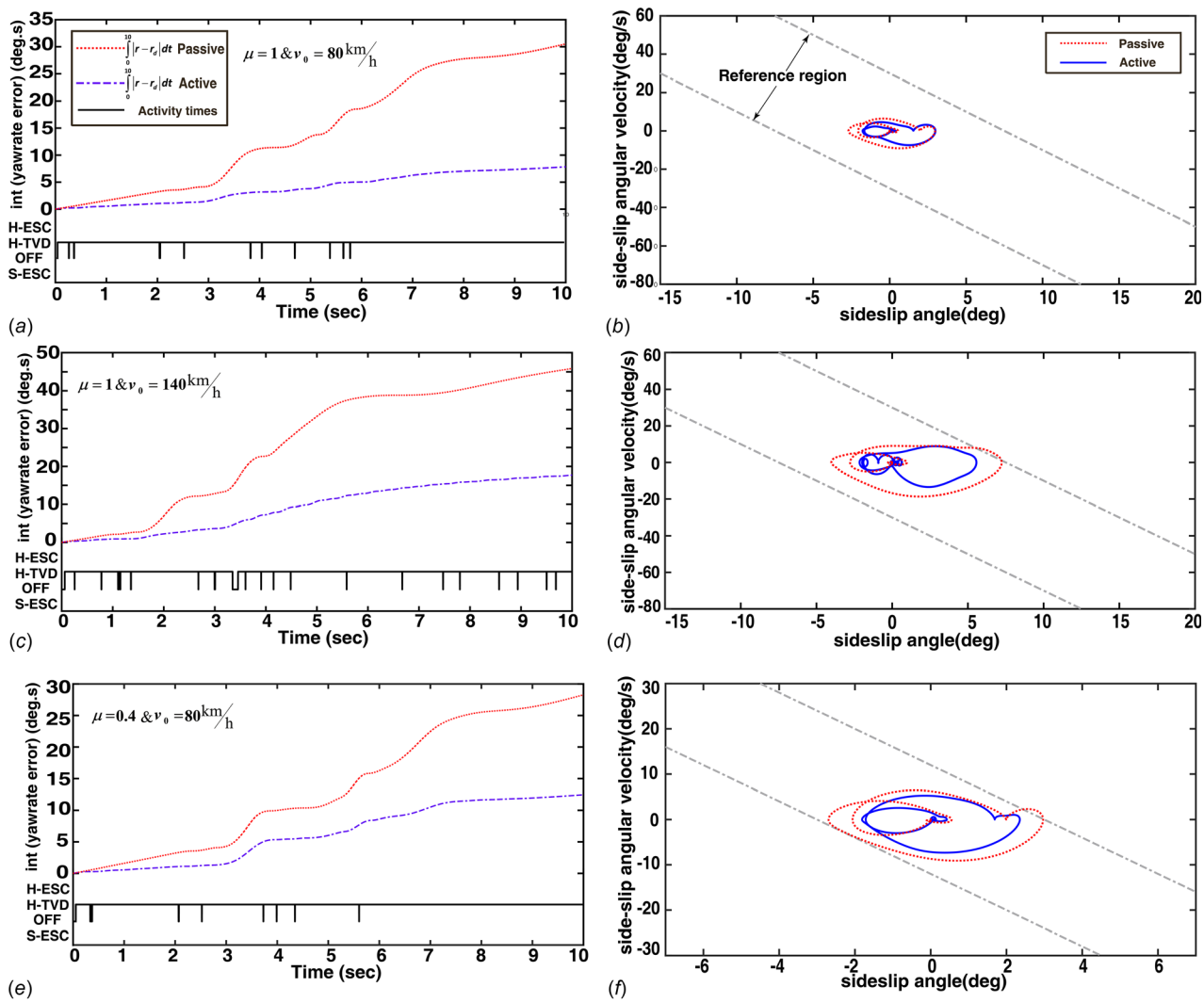

Fig. 10 Yaw rate error and the $\beta - \dot{\beta}$ phase trajectory in the phase plane in DLC

Downloaded From: https://dynamicsystems.asmedigitalcollection.asme.org on 11/20/2018 Terms of Use: http://www.asme.org/about-asme/terms-of-use

To assess the effectiveness and robustness of the proposed state estimator, the developed algorithms are tested in a variable road friction condition and $v_0 = 60\,\text{kph}$, $\delta_f = 5\,\text{deg}$. Figure 6 shows the estimated and actual values of vehicle parameters. It is seen from Fig. 6 that the estimated states are quite close to the simulation results.

6 Optimization

In order to improve the controller performances, the designed controller is optimized using BA optimization method. The BA method is an optimization algorithm, which is inspired from a searching behavior of the bees. The flowchart of BA algorithm is depicted in Fig. 7. In this method, a population of optimization parameters (fuzzy rules and the orientation of the membership functions) with n individuals, each called a bee, is generated. The cost function for each bee is evaluated to show which one finds better place for flowers. Comparing fitness function of the bees, m best places are selected and a ngh neighborhood for each m places is defined. Then a number of bees for best e places are recruited. After that, m bees related to the best m places are selected. For n-m remaining places, again some neighborhood is randomly defined and new population is generated.

Since the main purpose of controller is to improve the vehicle handling and vehicle stability, the objective function is obtained from the following equation:

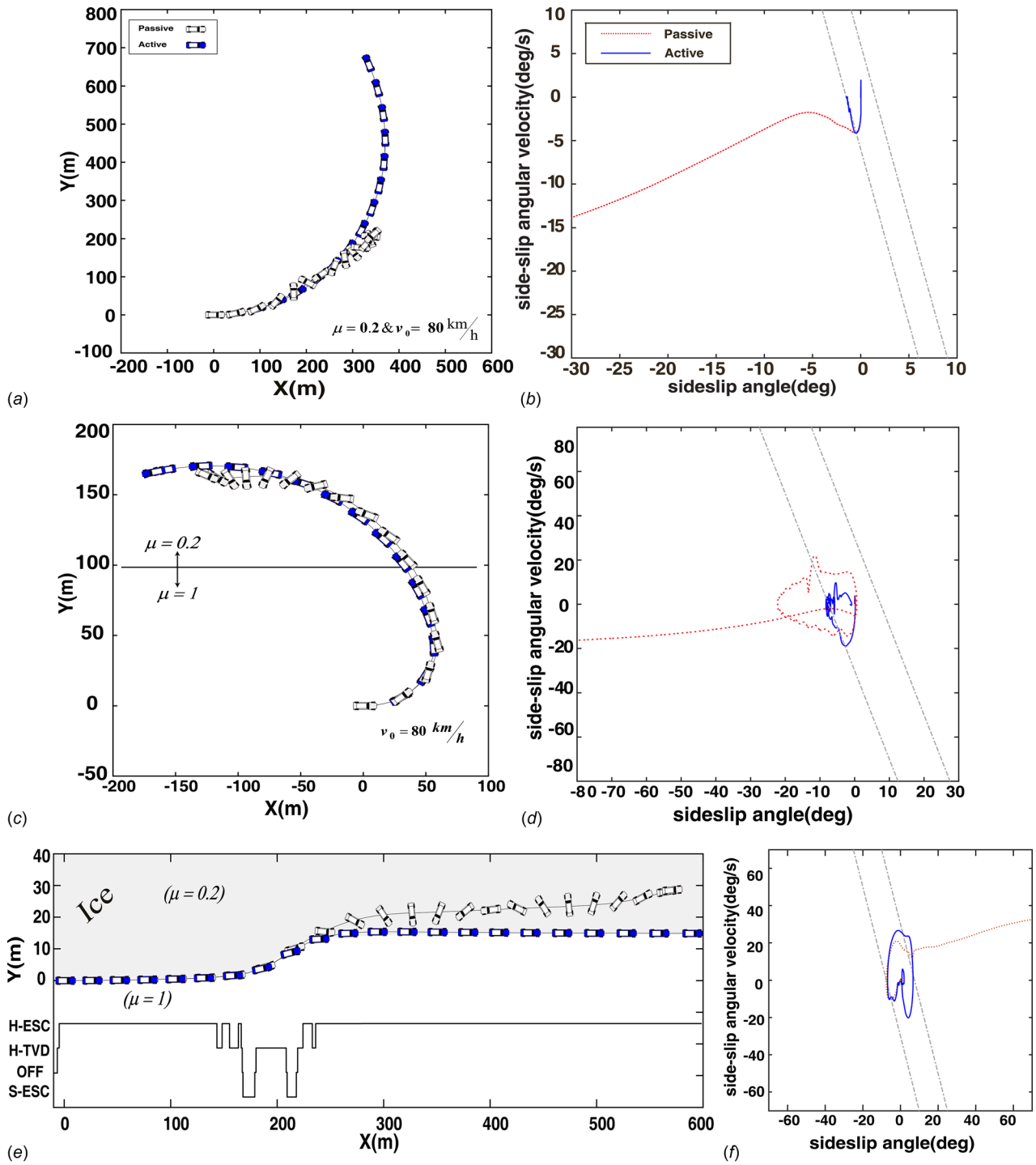

Fig. 11 Vehicle path and the $\beta - \dot{\beta}$ phase trajectory in the phase plane in different μ conditions

Downloaded From: https://dynamicsystems.asmedigitalcollection.asme.org on 11/20/2018 Terms of Use: http://www.asme.org/about-asme/terms-of-use

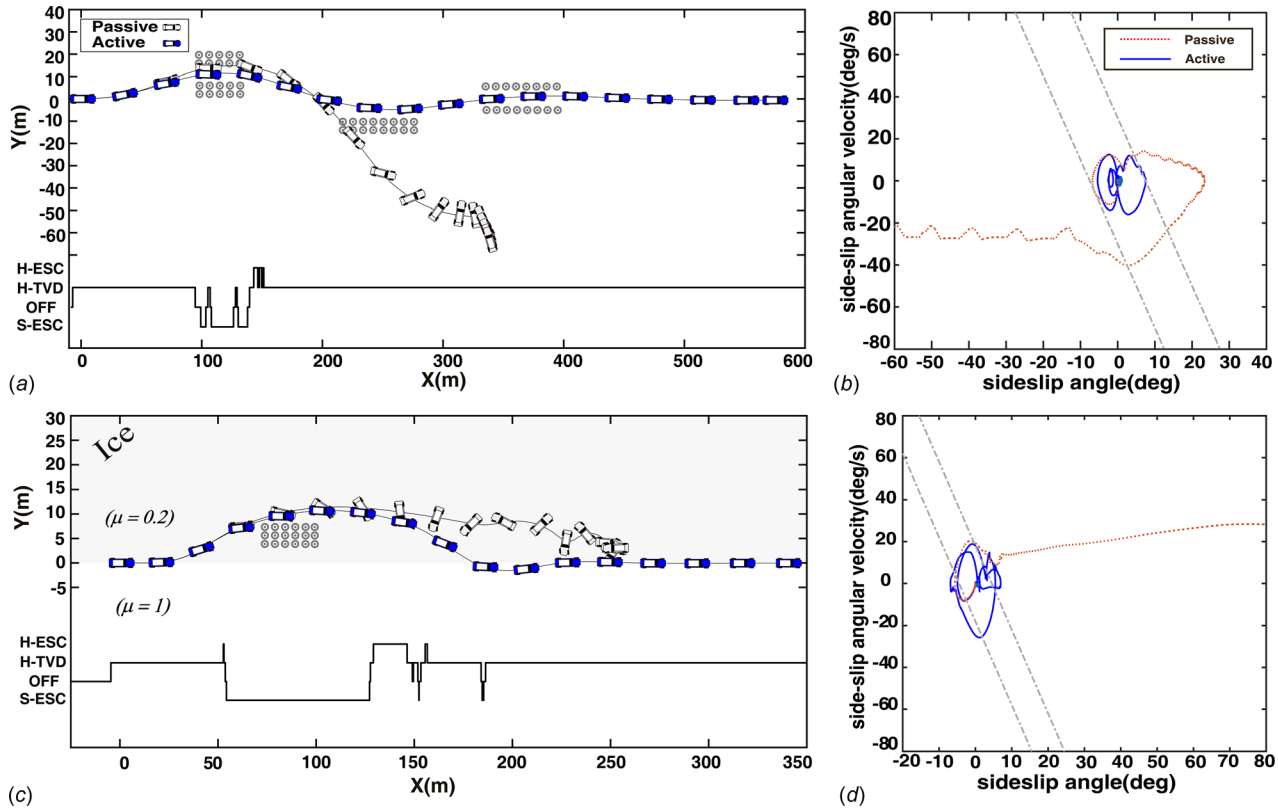

Fig. 12 Vehicle path and the $\beta-\dot{\beta}$ phase trajectory in the phase plane in critical situation

$$\text{minimize } F(u)$$
$$\text{where } F(u) = v_1 \int |r - r_d| \mathrm{d}t + v_2 \int |\xi| \mathrm{d}t \tag{27}$$

in which v_1 and v_2 are weight factors for normalization of cost function parameters. The first term of cost function is defined for minimizing the integral of yaw rate error ($e = r - r_d$) and the second term is define for minimizing the perpendicular distance of the actual state of the vehicle from the reference region in the phase plane (ξ) as much as possible. There are two layers of optimization. In the first layer, fuzzy rules are optimized. In the second layer, the skewness of the membership functions is taken to obtain best value of the cost function during a standard maneuver.

7 Discussion

In order to assessing the effectiveness of integrated control system, the performance of controller is investigated under different conditions including: (1) nearly normal and steady-state driving conditions, (2) different μ conditions, and (3) under critical situations.

7.1 Steady-State Conditions. In this section, standard test maneuvers, including the fishhook and double lane change (DLC), are considered and performed in low and high initial speed in dry and wet road conditions. Desired path in double lane change maneuver and the steering angle time history for the front wheels fishhook maneuver are shown in Figs. 8(*a*) and 8(*b*), respectively. Figures 9 and 10 show the integral of yaw rate error and the $\beta - \dot{\beta}$ phase trajectory in the phase plane in fishhook and DLC, respectively. Also, the activity times of each system are shown in these figures, where H-ESC means activated ESC for handling and inactive TVD, H-TVD means activated TVD for handling and inactive ESC, S-ESC means activated ESC for stability and inactive TVD and OFF means both systems are inactive. As can be seen, the integrated control system has improved the yaw rate while the vehicle side-slip angle has stayed in stable region.

7.2 Lower and Different μ Conditions. In this section, the robustness of integrated control system is evaluated under different road conditions. For this purpose, vehicle testing was performed on three surfaces; low μ in J-Turn maneuver, abrupt μ changes in J-Turn maneuver and split μ surface. Steering angle time history for the front wheels in J-Turn maneuver is shown in Fig. 8(*b*). In split μ surface, the friction coefficient between the left and right side of the road is quite different. This situation can be happened when the road itself has a high level of friction but the road banks are covered with snow or ice. Figure 11 shows the vehicle path and the $\beta - \dot{\beta}$ phase trajectory in the phase plane under low μ (Figs. 11(*a*) and 11(*b*)), abrupt μ changes (Figs. 11(*c*) and 11(*d*)), and split μ (Figs. 11(*e*) and 11(*f*)) conditions. As can be seen from Fig. 11, the integrated control system is robust against the road surface variations. A simple driver model was employed to control the steering wheel of the vehicle to follow the desired path.

7.3 Stability in Critical Situation. In order to demonstrate the effectiveness of integrated control system in the critical situation, two severe maneuvers are designed as discussed in Ref. [13].

At first maneuver, the vehicle faces unexpected obstacles and the vehicle should avoid them while its initial speed is high such that a passive vehicle loses its stability as shown in Fig. 12(*a*) ($v_0 = 140$ kph and max $\delta_f = 10$ deg) and the second one is a maneuver in which a passive vehicle starts to slip on a slippery road surface as shown in Fig. 12(*b*) ($v_0 = 80$ kph and max $\delta_f = 6$ deg). Same as Sec. 7.2, a simple driver model was employed to control the steering wheel of the vehicle to follow

Downloaded From: https://dynamicsystems.asmedigitalcollection.asme.org on 11/20/2018 Terms of Use: http://www.asme.org/about-asme/terms-of-use

the desired path. It is obviously seen that the integrated control system effectively improves stability in these situations.

8 Conclusion

In this paper, a full vehicle state estimation and an integrated TVD/ESC control strategy are proposed and tested under various driving conditions. For this purpose, a vehicle dynamics model of the 2003 Ford Expedition was developed in CarSim and an integrated control system between ESC and TVD was added to the vehicle model via MATLAB/SIMULINK. To control the integrated control system, a unified controller with three control layers based on fuzzy control strategy and $\beta - \dot{\beta}$ phase plane was designed. Based on the extended use of the $\beta - \dot{\beta}$ phase plane, the controller can switch between handling and stability control strategies. To detect the control parameters, a state estimator was developed based on UKF, which is a nonlinear estimator. In order to improve the controller performances, the fuzzy controller rules are optimized using Bees Algorithm. All simulations were performed using a co-simulation between the fully nonlinear Ford 2003 CarSim model and MATLAB/SIMULINK. The simulation results show that the integrated control system of ESC and TVD effectively improves the vehicle handling and stability in all tested regular and severe conditions. Actually, TVD in nearly normal conditions has the advantage to improve handling without having a significant negative effect on the longitudinal vehicle dynamics and ESC in critical conditions has the advantage to guarantee the vehicle stability.

Nomenclature

H-ESC = handling-ESC is activated to improve handling and TVD is inactive
H-TVD = handling-TVD is activated to improve handling and ESC is inactive
S-ESC = stability-ESC is activated to improve stability and TVD is inactive

Symbols

a, b = longitudinal distance from the front and rear axle to the center of mass, m
a_x, a_y = longitudinal and lateral accelerations, m s^{-2}
C_f, C_r = front/rear cornering stiffness, N rad^{-1}
F_{Li}, F_{Ci}, F_{zi} = longitudinal, lateral and vertical tire forces labeled $i = \mathrm{RF, LF, RR, LR}$, N
h = height of the mass center, m
I_{C1} = the moment of inertia of the left clutch, kg/m^2
I_{C2} = the moment of inertia of the right clutch, kg/m^2
I_i = the moment of inertia of the rear propeller shaft, kg/m^2
$I_{r2} = I_{r1}$ = the moment of inertia of the gear 4, kg/m^2
$I_{s2} = I_{s1}$ = the moment of inertia of the gear 1, kg/m^2
$I_z.I_w$ = vehicle and wheel moment of inertia, kg/m^2
I_1, I_2 = the moment of inertia of the rear left and rear right half shafts, respectively, kg/m^2
M, m = total vehicle mass, kg
r, r_d = vehicle yaw rate and desired yaw rate, rad s^{-1}
t = wheel tread, m
T_{ti}, T_{Bi} = torque supplied to the wheels labeled $i = \mathrm{RF, LF, RR, LR}$, N·m
U_{wi}, V_{wi} = longitudinal and lateral wheel center velocities $i = \mathrm{RF, LF, RR, LR}$, m s^{-1}
v_x, v_y = longitudinal and lateral velocities, m s^{-1}
Z_i = the number of teeth of the gears 1–4 in Fig. 4 ($i = 1 \ldots 4$)
α_i = side-slip angle of the wheel labeled $i = \mathrm{RF, LF, RR, LR}$
δ_f, δ = steering angle of front wheels, rad
ξ = perpendicular distance of vehicle state from the reference region
κ_i = longitudinal slip of wheel $i = \mathrm{RF, LF, RR, LR}$
μ = road friction coefficient
ω_1, ω_2 = angular velocity of the rear left and rear right wheels, respectively, rad s^{-1}
ω_i = angular velocity of the wheel labeled $i = \mathrm{RF, LF, RR, LR}$, rad s^{-1}

Appendix A

Numerical values of the active differential parameters are given in Table 1.

Table 1 Numerical values of the STC-TVD mechanism parameters [27]

$I_i^* = 0.15(\mathrm{kg/m^2})$	$h_1 = h_2 = 1.125$	$H_{11} = H_{21} = 4.5$
$H_{12} = H_{22} = 3.5$	$I_{c1} = I_{c2} = 0.002(\mathrm{kg/m^2})$	$I_{r1} = I_{r2} = 0.001(\mathrm{kg/m^2})$
$i = 2.8$	$I_3 = I_4 = 0.05(\mathrm{kg/m^2})$	$I_1 = I_2 = 0.05(\mathrm{kg/m^2})$

Appendix B

To set the fuzzy controller, a Gaussian membership function, Mamdani inference engine, and center of gravity defuzzification method have been employed. Table 2 shows performance of the controller in selecting the appropriate clutching or braking in TVD and ESC. Positive fuzzy output, means generating positive yaw moment, and the negative one, means the yaw moment is negative. Input and output normalized membership functions are shown in Figs. 13(*a*) and 13(*b*). Fuzzy rules used to control the torque control systems are given in Table 3. Where N, Z, and P

Table 2 Performance of the control system's third layer for handling and stability improvement

Handling	Error	δ_f	Fuzzy output	Vehicle status	TVD Clutching	ESC Braking
	$e < 0$	$\delta_f > 0$	Positive	Understeer	Right clutch	Rear-left
	$e < 0$	$\delta_f < 0$	Positive	Oversteer	Right clutch	Front-left
	$e > 0$	$\delta_f > 0$	Negative	Oversteer	Left clutch	Front-right
	$e > 0$	$\delta_f < 0$	Negative	Understeer	Left clutch	Rear-right

Stability	$\varepsilon_{\beta\dot{\beta}}$	Fuzzy output	δ_f	ESC Braking
	Negative	Negative	$\delta_f > 0$	Front-right
	Negative	Negative	$\delta_f < 0$	Rear-right
	Positive	Positive	$\delta_f > 0$	Rear-left
	Positive	Positive	$\delta_f < 0$	Front-left

Downloaded From: https://dynamicsystems.asmedigitalcollection.asme.org on 11/20/2018 Terms of Use: http://www.asme.org/about-asme/terms-of-use

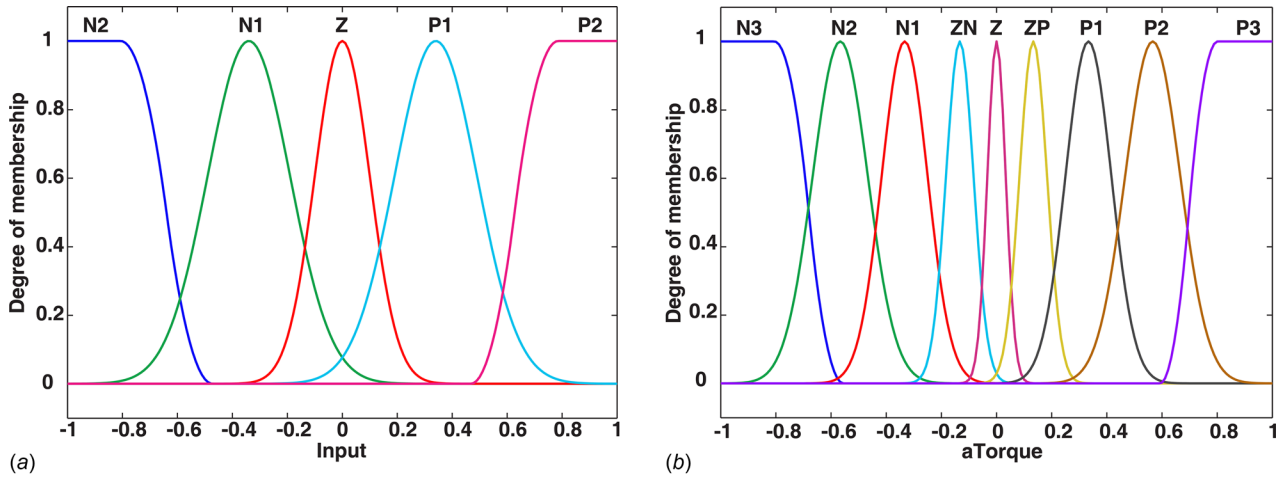

Fig. 13 (*a*) Input membership functions and (*b*) output membership functions for the fuzzy controller

Table 3 Fuzzy rule base for handling and stability

	Error / d/dt error	N2	N1	Z	P1	P2
Handling	N2	P3	P2	P1	ZP	Z
	N1	P2	P1	ZP	Z	ZN
	Z	P1	ZP	Z	ZN	N1
	P1	ZP	Z	ZN	N1	N2
	P2	Z	ZN	N1	N2	N3
Stability	N2	N3	N2	N1	ZN	Z
	N1	N2	N1	ZN	Z	ZP
	Z	N1	ZN	Z	ZP	P1
	P1	ZN	Z	ZP	P1	P2
	P2	Z	ZP	P1	P2	P3

mean negative, zero, and positive and 1, 2, 3 means medium, high, and very high and ZN and ZP mean negative low and positive low, respectively.

It should be added that when handling performance must be controlled, in oversteer situation the inside clutch of TVD system and in understeer the outside clutch of TVD system is activated but if the friction in the related tire is much lower than the other or the longitudinal slip in this tire is high or when the speed difference exceed at the allowable wheel speed difference or in very low road friction, this duty is relegate to ESC system. In ESC system, if $e < 0$ or $\varepsilon_{\beta\dot{\beta}} > 0$, braking force is applied on the inside rear wheel but if (1) this tire is on the threshold of locked mode, or (2) the friction in this tire is much lower than the inside front wheel or (3) when the longitudinal slip in this tire is high and in inside front wheel is low, then braking force is applied on the inside front wheel also in the situation in which $|\dot{\beta} + 4\beta| > 80\mu$ with considering the locked mode, longitudinal slip, and friction—as discussed above—braking force is applied on the both inside wheels. The same story is applied for $e > 0$ or $\varepsilon_{\beta\dot{\beta}} < 0$.

References

[1] Song, J., 2013, "Development and Comparison of Integrated Dynamics Control Systems With Fuzzy Logic Control and Sliding Mode Control," J. Mech. Sci. Technol., **27**(6), pp. 1853–1861.

[2] Wenzel, T. A., Burnham, K., Blundell, M., and Williams, R., 2006, "Dual Extended Kalman Filter for Vehicle State and Parameter Estimation," Veh. Syst. Dyn., **44**(2), pp. 153–171.

[3] Papelis, Y., Brown, T., Watson, G., Holtz, D., and Pan, W., 2004, "Study of ESC Assisted Driver Performance Using a Driving Simulator," University of Iowa's National Advanced Driving Simulator, Coralville, IA, Report No. N2004-030.

[4] Jaafari, S. M. M., and Shirazi, K. H., 2016, "A Comparison on Optimal Torque Vectoring Strategies in Overall Performance Enhancement of a Passenger Car," Proc. Inst. Mech. Eng., Part K: J. Multi-Body Dyn., **230**(4), pp. 469–488.

[5] Sawase, K., and Sano, Y., 1999, "Application of Active Yaw Control to Vehicle Dynamics by Utilizing Driving/Breaking Force," JSAE Rev., **20**(5), pp. 289–95.

[6] Piyabongkarn, D., Lew, J. Y., Rajamani, R., and Grogg, J. A., 2010, "Active Driveline Torque-Management Systems," IEEE Control Syst. Mag., **30**(4), pp. 86–102.

[7] Hancock, M., Williams, R., Gordon, T., and Best, M. C., 2005, "A Comparison of Braking and Differential Control of Road Vehicle Yaw-Sideslip Dynamics," Proc. Inst. Mech. Eng., Part D, **219**(3), pp. 309–327.

[8] He, J., Crolla, D., Levesley, M., and Manning, W., 2006, "Coordination of Active Steering, Driveline, and Braking for Integrated Vehicle Dynamics Control," Proc. Inst. Mech. Eng., Part D, **220**(10), pp. 1401–1420.

[9] Cooper, N. J., 2006, *Active Driveline and Suspension Control to Improve Vehicle Handling*, University of Leeds, Leeds, UK.

[10] Goodarzi, A., and Alirezaie, M., 2009, "Integrated Fuzzy/Optimal Vehicle Dynamic Control," Int. J. Automot. Technol., **10**(5), pp. 567–575.

[11] Mechanical Simulation Corporation, 2017, "CarSim," Mechanical Simulation Corporation, Ann Arbor, MI, accessed Dec. 15, 2017, https://www.carsim.com/

[12] Kinjawadekar, T., Dixit, N., Heydinger, G., Guenther, D., and Salaani, M. k., 2009, "Vehicle Dynamics Modeling and Validation of the 2003 Ford Expedition With ESC Using CarSim," SAE Paper No. 2009-01-0452.

[13] Jaafari, S. M. M., 2012, "Optimal Control of Torque Splitter System for a 4WD Vehicle for Better Handling," M.Sc. thesis, University of Ahvaz, Ahvaz, Iran.

[14] Mimura, K., 2005, "Differential Gear," U.S. Patent No. 6120407.

[15] Deur, J., Petric, J., Asgari, J., and Hrovat, D., 2005, "Modeling of Wet Clutch Engagement Including a Thorough Experimental Validation," SAE Paper No. 2005-01-0877.

[16] Hancock, M., 2006, "Vehicle Handling Control Using Active Differentials," Ph.D. thesis, University of Loughborough, Loughborough, UK.

[17] Karnopp, D., 1985, "Computer Simulation of Stick-Slip Friction in Mechanical Dynamic Systems," ASME J. Dyn. Syst., Meas., Control., **107**(1), pp. 100–103.

[18] Rajamani, R., 2005, *Vehicle Dynamics and Control*, 1st ed., Springer, New York, pp. 221–256.

[19] He, J., 2005, "Integrated Vehicle Dynamics Control Using Active Steering, Driveline and Braking," Ph.D. thesis, University of Leeds, Leeds, UK.

[20] Inagaki, S., Kushiro, I., and Yamamoto, M., 1995, "Analysis on Vehicle Stability in Critical Cornering Using Phase-Plane Method," JSAE Rev., **16**(2), p. 216.

[21] Smakman, H., 2000, *Functional Integration of Slip Control With Active Suspension for Improved Lateral Vehicle Dynamics*, Delft University of Technology, Delft, The Netherlands.

[22] Wong, J. Y., 2001, *Theory of Ground Vehicles*, 3rd ed., Willey, New York.

[23] Antonov, S., Fehn, A., and Kugi, A., 2011, "Unscented Kalman Filter for Vehicle State Estimation," Veh. Syst. Dyn., **49**(9), pp. 1497–1520.

[24] Pacejka, H. B., 2006, *Tire and Vehicle Dynamics*, 2nd ed., Butterworth-Heinemann, Oxford, UK.

[25] Julier, S. J., and Uhlmann, J. K., 1997, "A New Extension of the Kalman Filter to Nonlinear Systems," International Symposium on Aerospace/Defense Sensing, Simulations and Controls, Orlando, FL, Apr. 20–25, pp. 182–93.

[26] Rhudy, M., and Gu, Y., 2013, "Understanding Nonlinear Kalman Filters—Part II: An Implementation Guide," West Virginia University, Morgantown, WV, accessed Dec. 15, 2017, https://docgo.net/understandig-nonlinear-kalman-filters-part-ii-an-implementation-guide-copy

[27] Deur, J., Ivanović, V., Hancock, M., and Assadian, F., 2010, "Modeling and Analysis of Active Differential Dynamics," ASME J. Dyn. Syst., Meas., Control., **132**(6), p. 061501.

Downloaded From: https://dynamicsystems.asmedigitalcollection.asme.org on 11/20/2018 Terms of Use: http://www.asme.org/about-asme/terms-of-use